Electronic Supplementary Material (ESI) for Lab on a Chip.

Serial flow cytometry in an inertial focusing optofluidic microchip for direct assessment of measurement variations

Matthew DiSalvo,[a,c] Paul N. Patrone [b], Anthony J. Kearsley,[b] and Gregory A. Cooksey [c,] *

[a] Department of Mechanical Engineering, Johns Hopkins University, Baltimore, Maryland 21287, United States.
[b] Applied and Computational Mathematics Division, National Institute of Standards and Technology, Gaithersburg, Maryland 20899, United States.
[c] Microsystems and Nanotechnology Division, National Institute of Standards and Technology, Gaithersburg, Maryland 20899, United States.
* Corresponding author. Phone: (301) 975-5529, E-mail: gregory.cooksey@nist.gov.

Supplemental Figures and Video

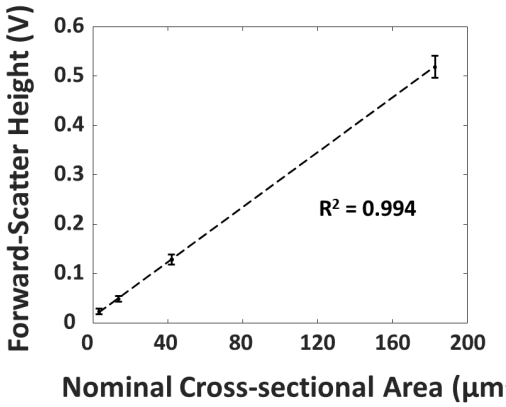

Fig. S1 Characterization of microcytometer forward scatter measurements using a microsphere size calibration ladder. Black points represent mean values; error bars represent ± 1 standard deviation; dashed line is a linear fit.

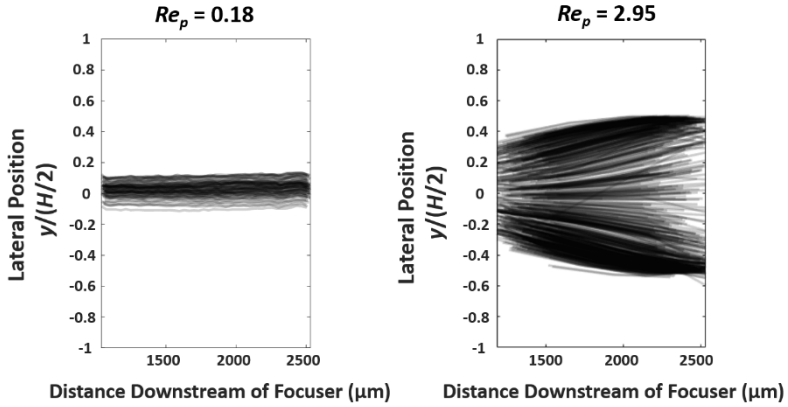

Fig. S2 Imaging characterization of lateral positions of 15.3 µm diameter polystyrene microspheres that were hydrodynamically focused to the channel centerline. The vertical axis is normalized such that 0 is the channel centerline and ± 1 are the vertical channel walls (corresponding to approximately 20 µm from the centerline). Traces indicate tracked microsphere intensity-weighted centroids. Darker shading indicates high local trace density.

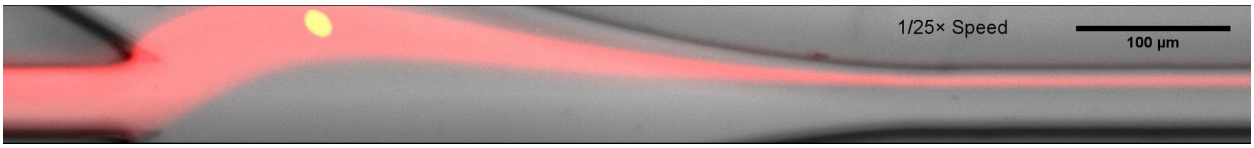

Supplemental Video Hybrid inertial and hydrodynamic particle focusing by biased sheath flow at a cross-junction. The video (still-frame shown above, see ESI for video file) shows the motion of fluorescent polystyrene microspheres (green), which is composited onto a static image of the microchannels (gray) and fluorescently labeled core fluid (red). The videoframes that did not contain a microsphere have been removed. Accelerating microspheres appear as slanted ovals due to a motion blur effect resulting from the camera sequentially scanning rows of pixels. Sheath fluid (unlabeled) enters this cross-junction from above and below; for more details, refer to Fig. 3B of the main text. Video speed is 25 times slower than actual speed.

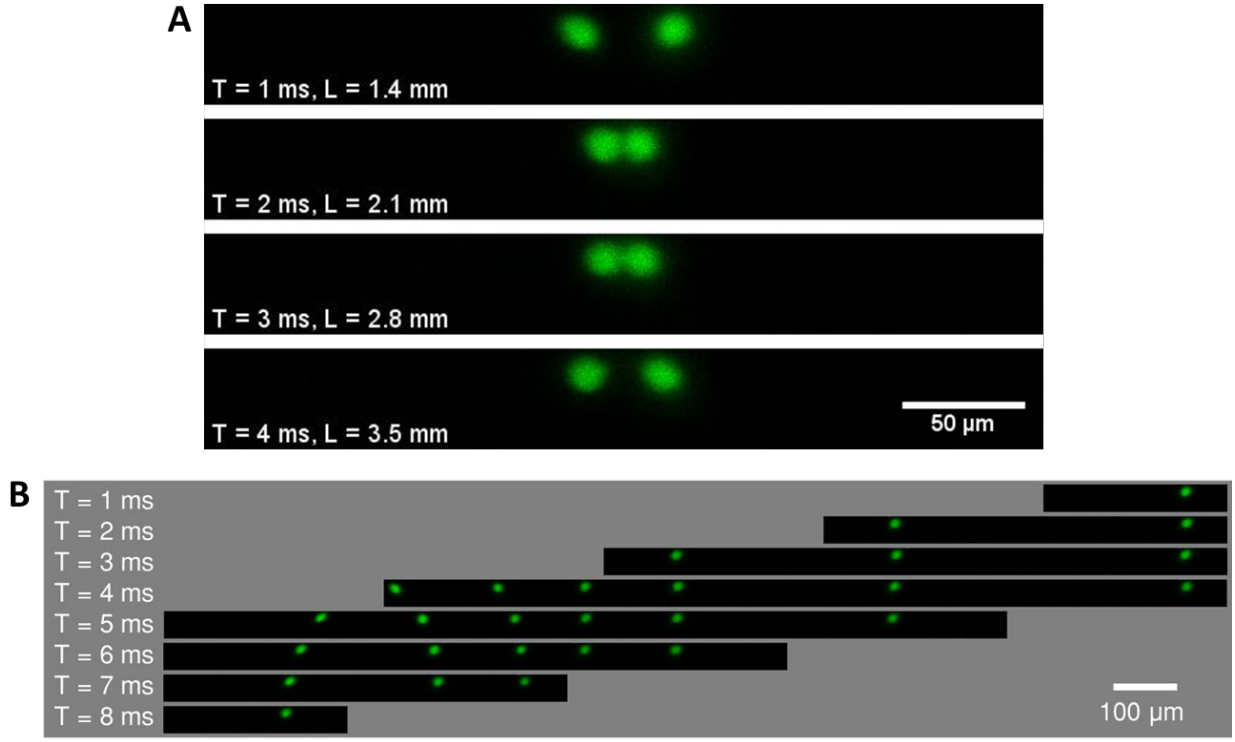

Fig. S3 Particle-particle interactions of flowing particles at $Re_p \approx 3$. Fluorescence microscopy images of A) dynamic interaction between two particles and B) interactions within a train of particles. Flow is from left to right, and the images have been translated to account for the particle motion between frames. The microchannel walls (not visible) are located along the horizontal border of each image strip. Particles were pre-positioned towards the upper channel wall at flow length $L = 0$ mm using approximately a 6 : 1 bias of sheath flows, and the images were recorded at $L \approx 2$ mm. Accelerating/decelerating microspheres appear as slanted ovals due to a motion blur effect resulting from the camera sequentially scanning rows of pixels.

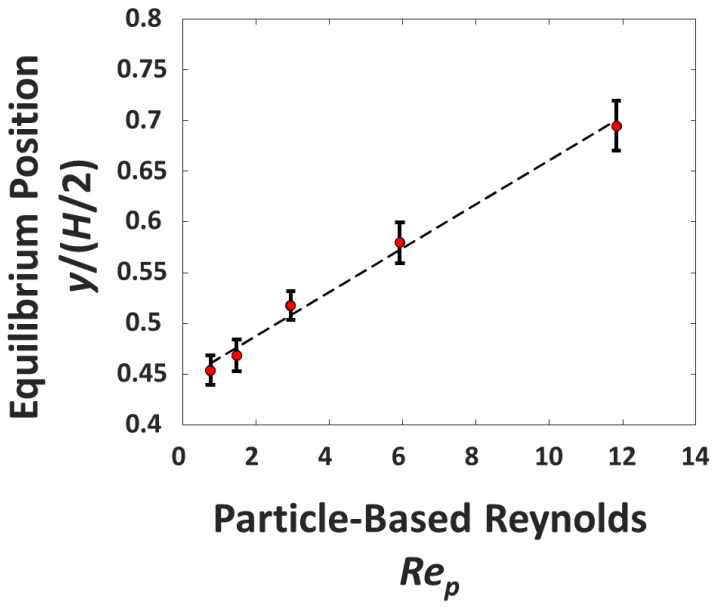

Fig. S4 Image-based characterization of lateral inertial equilibration positions of 15.3 µm diameter polystyrene microspheres. Particle velocities were varied by adjusting total volumetric flow rates through the microfluidic cytometer with hybrid inertial particle focusing. The vertical axis is normalized such that 0 is the channel centerline and ± 1 are the vertical channel walls (corresponding to approximately 20 µm from the centerline). Red points represent mean particle centroids; error bars represent ± 1 standard deviation; dashed line is a linear fit.

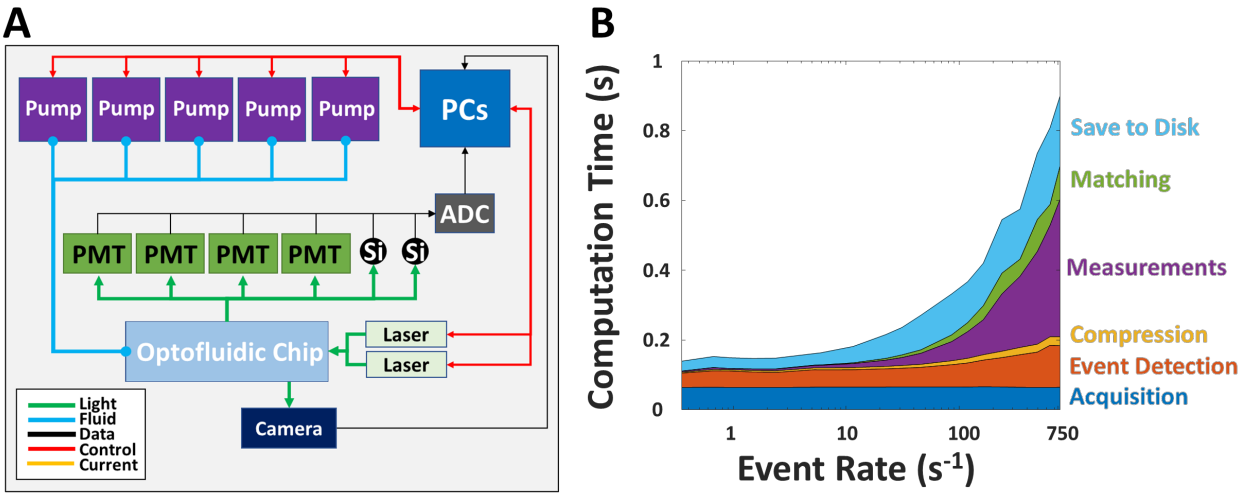

Fig. S5 Serial cytometer automation. A) Instrumentation schematic. "Si": Silicon photodetector; "ADC": Analog-to-digital converter. B) Real-time computation speeds for serial cytometry data acquisition and analysis. The acquisition interval was normalized to 1 s.

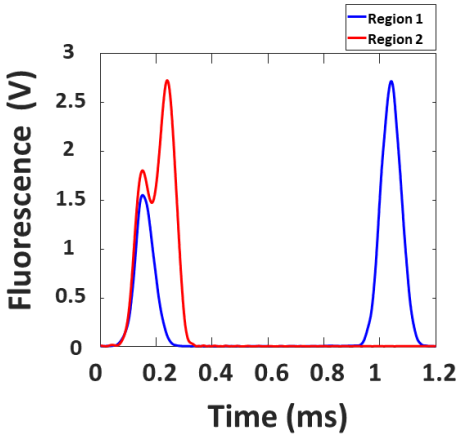

Fig. S6 Challenges for particle tracking. Measurement of 2 separated particles at region 1 (blue trace) appear well separated at region 1 but have reached close proximity at region 2 (red trace) and thus appear as an overlapping signal, or doublet. Traces are shown aligned in time relative to a brief window of background collected prior to reaching a detection threshold voltage (as indicated in Figure 2C). Such data were counted as mismatches and were not included in reproducibility statistics.

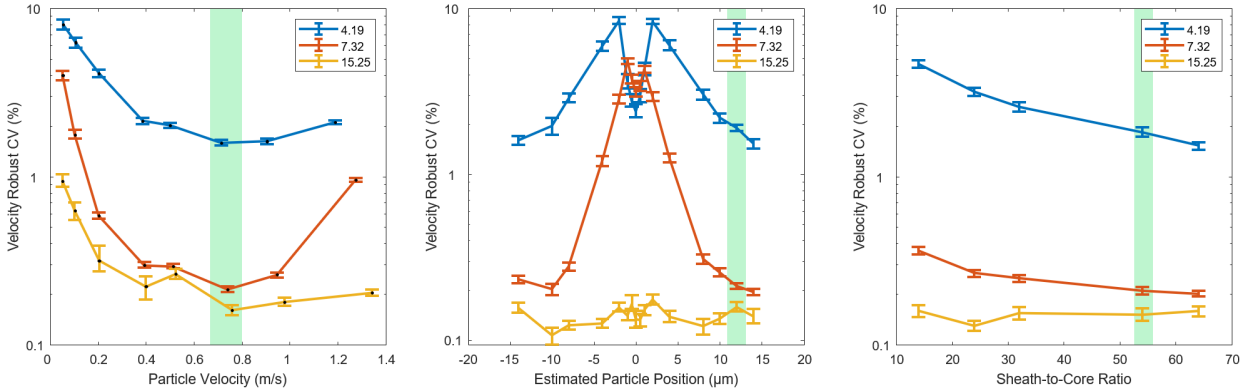

Fig. S7 Particle population variation in velocity using the hybrid focusing serial cytometer. Error bars indicate a 95 % confidence interval from bootstrap analyses. The legend lists particle diameter, in µm. The green bands indicate a flow condition in common across the three parameter screens (velocity: 0.75 m/s; particle position: 12 µm equivalent to $y_{core}/(H/2)$: 0.6; SCR: 54).

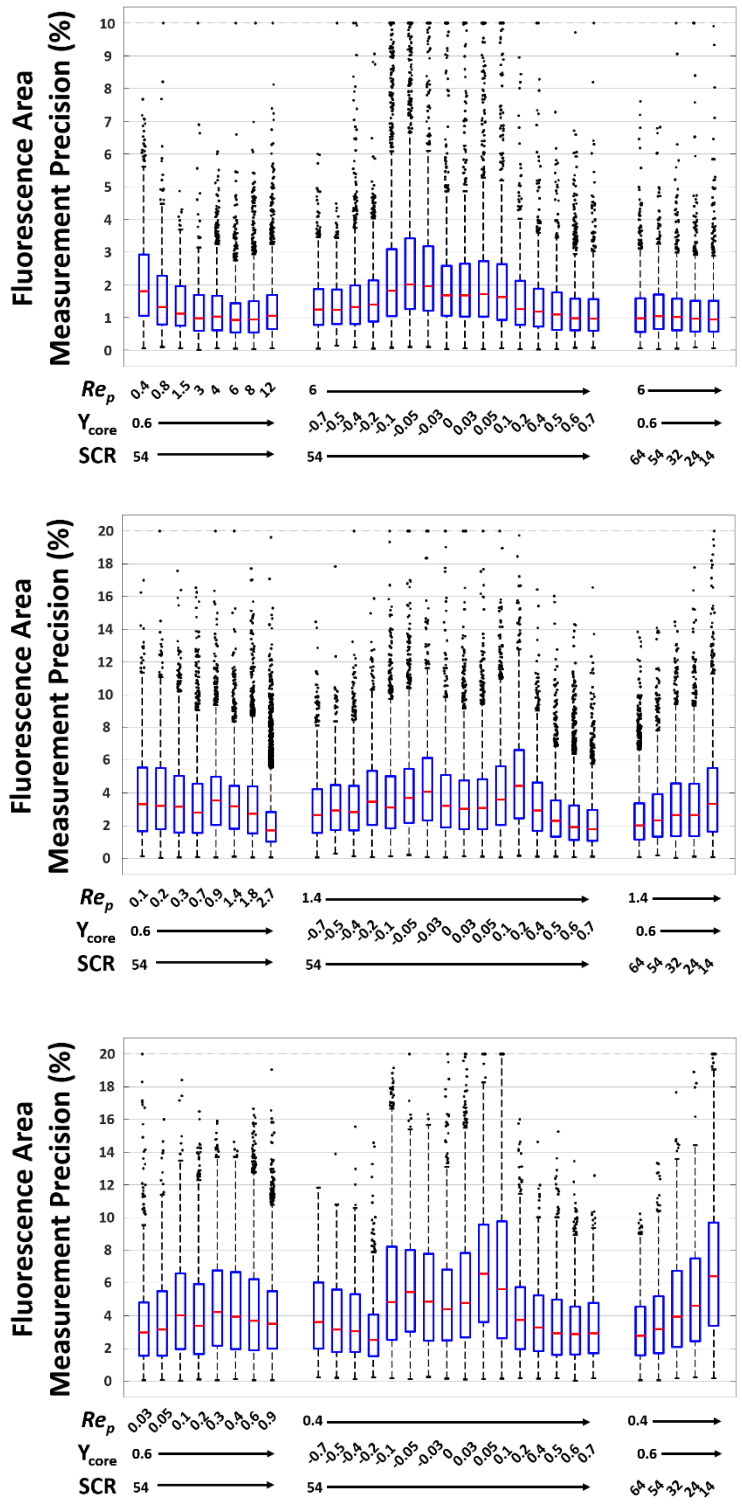

Fig. S8 Full results showing refinement of measurement precision. Box-and-whisker plots illustrating the screening of precision in fluorescence measurements of 15 µm (top), 7 µm (middle), and 4 µm (bottom) fluorescence particles through sequential evaluation of three flow parameters: Re_p, y_{core}, and then *SCR*. Blue boxes represent the interquartile range (IQR); red lines indicate the median; dashed black lines extend 1.5 × IQR. For visibility, the y-axis is clipped at the dashed horizontal lines and only outlier datapoints are individually drawn.

Table S1 Flow rates and targeted parameters for screen study.

Volumetric Flow Rates (µL/min)					Velocity (m/s)	$y_{core}/(H/2)$	*SCR*
Right Sheath	Left Sheath	Sample	Upper Sheath	Lower Sheath			
5.3	0.7	0.1	0.6	0.6	0.05	0.6	54
10.6	1.4	0.3	1.3	1.3	0.1	0.6	54
21.2	2.7	0.5	2.5	2.5	0.2	0.6	54
42.4	5.4	1.1	5.1	5.1	0.4	0.6	54
56.5	7.3	1.4	6.8	6.8	0.5	0.6	54
84.7	10.9	2.1	10.2	10.2	0.75	0.6	54
112.9	14.5	2.9	13.6	13.6	1	0.6	54
169.4	21.8	4.3	20.4	20.4	1.35	0.6	54
6.5	89.1	2.1	10.2	10.2	0.75	-0.7	54
18.3	77.3	2.1	10.2	10.2	0.75	-0.5	54
24.2	71.4	2.1	10.2	10.2	0.75	-0.4	54
36.0	59.6	2.1	10.2	10.2	0.75	-0.2	54
41.9	53.7	2.1	10.2	10.2	0.75	-0.1	54
44.8	50.7	2.1	10.2	10.2	0.75	-0.05	54
46.3	49.3	2.1	10.2	10.2	0.75	-0.025	54
47.8	47.8	2.1	10.2	10.2	0.75	0	54
49.3	46.3	2.1	10.2	10.2	0.75	0.025	54
50.8	44.8	2.1	10.2	10.2	0.75	0.05	54
53.7	41.9	2.1	10.2	10.2	0.75	0.1	54
59.6	36.0	2.1	10.2	10.2	0.75	0.2	54
71.4	24.2	2.1	10.2	10.2	0.75	0.4	54
77.3	18.3	2.1	10.2	10.2	0.75	0.5	54
83.2	12.4	2.1	10.2	10.2	0.75	0.6	54
89.1	6.5	2.1	10.2	10.2	0.75	0.7	54
85.6	11.8	1.8	9.5	9.5	0.75	0.6	64
84.7	10.9	2.1	10.2	10.2	0.75	0.6	54
81.4	7.6	3.6	12.7	12.7	0.75	0.6	32
79.2	5.4	4.7	14.3	14.3	0.75	0.6	24
74.4	0.6	7.9	17.6	17.6	0.75	0.6	14